Spin-polarization anisotropy in a narrow spin-orbit-coupled nanowire quantum dot

M. P. Nowak and B. Szafran
AGH University of Science and Technology, Faculty of Physics and Applied Computer Science, al. Mickiewicza 30, 30-059 Kraków, Poland

(Received 29 October 2012; revised manuscript received 29 April 2013; published 24 May 2013)

One- and two-electron systems confined in single and coupled quantum dots defined within a nanowire with a finite radius are studied in the context of spin-orbit coupling effects. The anisotropy of the spin-orbit interaction is discussed in terms of the system geometry and orientation of the external magnetic field vector. We find that there are easy and hard spin-polarization axes, and in the quantum dot with strong lateral confinement electron spin becomes well defined in spite of the presence of spin-orbit coupling. We present an analytical solution for the one-dimensional limit and study its validity for nanowires of finite radii by comparing the results with a full three-dimensional calculation. The results are also compared with the recent measurements of the effective Landé factor and avoided crossing width anisotropy in InSb nanowire quantum dots [S. Nadj-Perge *et al.*, Phys. Rev. Lett. **108**, 166801 (2012)].

DOI: 10.1103/PhysRevB.87.205436 PACS number(s): 73.21.La, 71.70.Gm

I. INTRODUCTION

There is a growing interest in gated semiconductor nanowires in the context of possible applications for spin-operating devices.[1–4] These structures provide a good basis for the creation of small electrostatic quantum dots with confinement introduced by external potentials. Energy spectra of such dots as determined[5] by transport spectroscopy bear distinct signatures of strong spin-orbit (SO) interaction which results from the structure inversion asymmetry (Rashba SO coupling[6]) or the bulk inversion asymmetry (Dresselhaus SO interaction[7]). SO coupling mixes spin and orbital degrees of freedom, thus opening the possibility of fully electrical control of the electron spin.[1–4,8,9] Moreover, SO coupling allows for electron spin relaxation mediated by phonons,[10,11] and introduces anisotropic corrections to spin exchange interaction for electrons in double quantum dots.[12]

The SO coupling opens avoided crossings[5] in the quantum dot energy spectra as a function of the external magnetic field (**B**). The width of the avoided crossings between energy levels of different spin states depends on the orientation of the **B** vector, which reveals the spatial anisotropy of the SO interaction.[3,13–15] Moreover, the mixing of the spin states by SO coupling determines an effective Landé factor (g factor) and its anisotropy[16] as a function of the magnetic field orientation. In nanowire quantum dots the effective g-factor was recently measured in electric dipole spin resonance (EDSR) experiments[2,3] for a two-electron spin-blocked configuration or by magnetotransport measurements on electron[17] and hole[18] quantum dots. The anisotropy of SO interaction is a relevant issue for spin qubit manipulation[1] as well as for helical spin liquids[19] which in the proximity of a superconductor can be used for observation of Majorana fermions.[20]

It is well known that in the presence of SO coupling, the electron spin can be well defined in the stationary eigenstates only for equal Rashba and Dresselhaus SO coupling constants.[21] This fact was exploited in a proposal of a nonballistic spin field effect transistor[21] and for the prediction[22] of a persistent spin helix.[23] In the present work, we demonstrate that in the limit of strong lateral confinement, the electron spins confined in the quantum dot become well defined in the direction perpendicular to the wire axis and the external electric field vector in spite of the presence of the Rashba coupling. We show that in a general case, the extent of the electron spin polarization strongly depends on the orientation of **B** reflecting the anisotropy of SO interaction.

For a description of narrow nanowires, a one-dimensional model is commonly used.[24] In this work, we present an analytical form of eigenstates for this approximation for a quantum dot defined in a nanowire. The analytical form of the SO-coupled wave functions accounts for the anisotropic spin polarization and explains the different strengths of the spin-splittings for varied orientation of the magnetic field. We study the applicability of the one-dimensional model for a nanowire with a finite radius by comparing its results with the three-dimensional calculation for various geometries of the nanowire quantum dot. To relate the model results to the experimental measurements, we study coupled two-electron quantum dots, i.e., the configuration that is used for EDSR and the spin exchange experiments. The obtained shape of the g factor and the avoided crossing width dependence on magnetic field orientation resemble the findings of the experiment of Ref. 3 on InSb nanowire quantum dots.

II. THEORY

We consider a single-electron quantum dot defined in a narrow nanowire described by the three-dimensional Hamiltonian

$$h = \frac{\hbar^2\mathbf{k}^2}{2m^*} + V(\mathbf{r}) + H_{\mathrm{SO}} + \frac{1}{2}g\mu_B\mathbf{B}\cdot\sigma, \qquad (1)$$

where $\mathbf{k} = -i\nabla + e\mathbf{A}/\hbar$ with the gauge $\mathbf{A} = B(z\sin\phi, 0, y\cos\phi)$. The magnetic field is aligned in the xy plane with an angle ϕ between **B** and the x axis—in such a case, the Zeeman term stands for $\frac{1}{2}g\mu_B\mathbf{B}\cdot\sigma = \frac{1}{2}\mu_B g B(\sigma_x\cos\phi + \sigma_y\sin\phi)$, $V(\mathbf{r})$ stands for the confinement potential which we take in a separable form $V(\mathbf{r}) = V_l(y,z) + V_L(x) + |e|\mathbf{F}\cdot\mathbf{r}$, where $V_l(y,z)$ is a 400-meV-deep two-dimensional circular quantum well of radius R, $V_L(x)$ is an infinite quantum well with width L (see Fig. 1), and **F** stands for the external electric field. We account

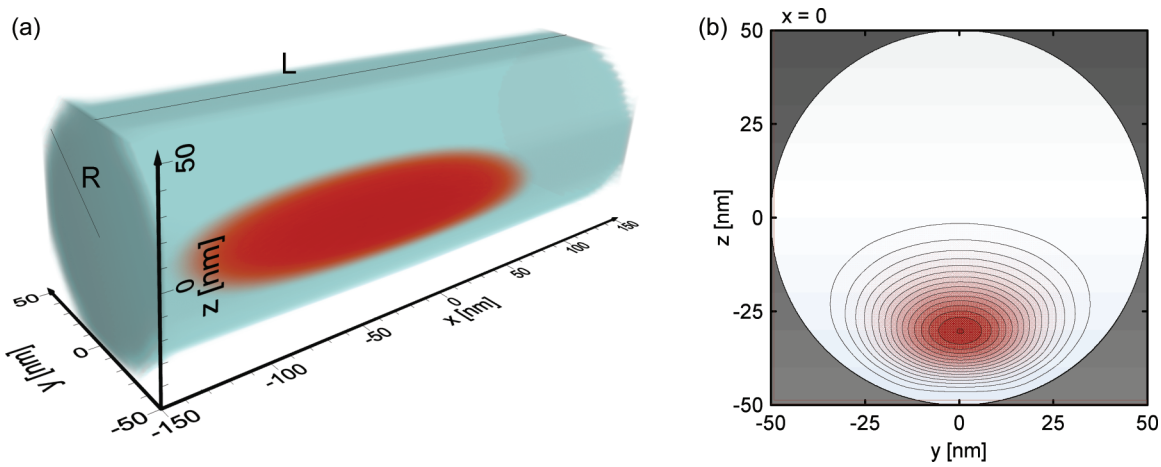

FIG. 1. (Color online) (a) Sketch of the confinement potential $V(\mathbf{r})$ of the nanowire quantum dot (with blue) and the single-electron charge density (with red) calculated for $F_z = 10$ kV/cm. (b) Cross section of the confinement potential and the charge density for $x = 0$.

for Rashba SO coupling $H_{\rm SO} = \alpha_0 \frac{\partial V}{\partial r} \cdot (\sigma \times \mathbf{k})$ as the main SO interaction type in the [111] grown InSb nanowires.[3] Unless stated otherwise, we assume the electric field $\mathbf{F} = (0,0,F_z)$ with a nonzero component in the z direction (perpendicular to the axis of the wire) due to the gating of the nanowire.[1–4] We assumed a hard-wall confinement potential of the wire. The electron wave function vanishes at the edge of a circular quantum well $V_l(y,z)$ [see Fig. 1(b)]. Therefore, the only part of the potential whose gradient overlaps with the wave function and thus gives rise to the SO coupling is the external electric potential, i.e., $H_{\rm SO} = \alpha(\sigma_x k_y - \sigma_y k_x)$, where $\alpha = \alpha_0 F_z$.

To solve the Schrödinger equation, we rewrite the Hamiltonian Eq. (1) as $h = h_x + h_y + h_z + h_{ns}$, where

$$h_x = -\frac{\hbar^2}{2m^*}\frac{\partial^2}{\partial x^2} + V_L(x), \tag{2}$$

$$h_y = -\frac{\hbar^2}{2m^*}\frac{\partial^2}{\partial y^2} + V_B(y) + \frac{e^2B^2}{2m^*}y^2\cos^2\phi, \tag{3}$$

$$h_z = -\frac{\hbar^2}{2m^*}\frac{\partial^2}{\partial z^2} + V_B(z) + \frac{e^2B^2}{2m^*}z^2\sin^2\phi + |e|F_z z, \tag{4}$$

are separable in the x-, y-, and z-direction spin-independent parts. The infinite quantum wells $V_B(y)$ and $V_B(z)$ of width $2R$ define the computational box, and

$$h_{ns} = -\frac{i\hbar eB}{m^*}\left(z\sin\phi\frac{\partial}{\partial x} + y\cos\phi\frac{\partial}{\partial z}\right) + \frac{1}{2}g\mu_b B[\sigma_x\cos\phi + \sigma_y\sin\phi] + H_{\rm SO} + V_l(y,z) \tag{5}$$

is the nonseparable part that contains the spin dependency and the potential of the cylindrical quantum well $V_l(y,z)$.

The calculation procedure proceeds as follows. We calculate eigenvectors of h_x, h_y, and h_z on meshes containing 1000 points and use them for construction of a basis (which consists of 8192 elements) in which the h Hamiltonian is diagonalized. As a result, we obtain three-dimensional spin orbitals $\psi(\mathbf{r},\sigma)$. Note that introducing the infinite quantum wells V_B in the first step fixes the basis for the diagonalization of the complete Hamiltonian.

The solutions of the two-electron system described by the Hamiltonian

$$H = h_1 + h_2 + \frac{e^2}{4\pi\varepsilon_0\varepsilon|\mathbf{r}_1 - \mathbf{r}_2|} \tag{6}$$

are found in the basis constructed from products of antisymmetrized single-electron spin orbitals $\psi(\mathbf{r},\sigma)$,

$$\Psi(\mathbf{r}_1,\sigma_1,\mathbf{r}_2,\sigma_2) = \frac{1}{\sqrt{2}}\sum_{i=1}^{M}\sum_{j=i+1}^{M} c_{ij}[\psi_i(\mathbf{r}_1,\sigma_1)\psi_j(\mathbf{r}_2,\sigma_2) - \psi_i(\mathbf{r}_2,\sigma_2)\psi_j(\mathbf{r}_1,\sigma_1)], \tag{7}$$

where the coefficients c_{ij} are found by diagonalization of Hamiltonian Eq. (6) according to the configuration interaction method with $M = 20$. The scheme treats the Coulomb interaction in an exact manner. For the calculation of the Coulomb matrix elements, we use the two-step method that replaces six-dimensional integrations by calculation of the Poisson equation for the potential generated from single-electron wave functions and integrate it with the product of the wave function of the other electron.[14]

We adopt material parameters[26] for InSb, namely $m^* = 0.014m_0$, $g = -51$, $\varepsilon = 16.5$, and $\alpha_0 = 5$ nm^2. In the bulk of the paper, we choose $F_z = 50$ kV/cm, which results in a SO interaction constant $\alpha = 25$ meV nm. Unless stated otherwise, we take $L = 300$ nm.

III. RESULTS

A. Single electron in a finite thickness nanowire quantum dot

The lowest part of the energy spectrum of the single-electron quantum dot is presented in Fig. 2. In the absence of the magnetic field, all the levels are Kramer's doublets. We include the residual magnetic field $B = 5$ mT and inspect the spin polarization along the magnetic field direction [calculated as $\langle s_B\rangle = \langle s_x\rangle\cos(\phi) + \langle s_y\rangle\sin(\phi)$]. In Fig. 3(a), we observe that the spin polarization undergoes oscillatory changes as a function of $\mathbf{B}$ orientation. This reflects the presence of easy and hard spin-polarization axes in the system. For the magnetic field oriented perpendicular to the nanowire axis, the spin

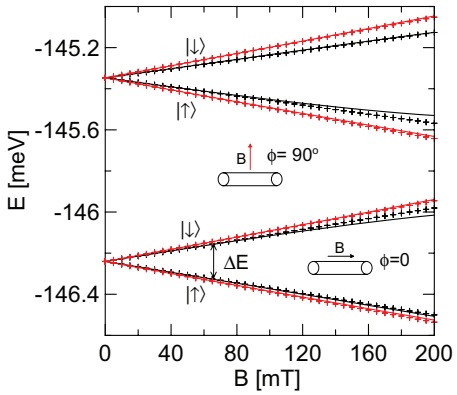

FIG. 2. (Color online) Single-electron energy spectrum for the SO coupled nanowire quantum dot with radius $R = 50$ nm and SO interaction constant $\alpha = 25$ meV nm plotted with lines for two orientations of the magnetic field. The crosses are the results obtained from the asymptotic one-dimensional solution—see the text. With $|\uparrow\rangle$ and $|\downarrow\rangle$ we mark the spin polarization of the states parallel and antiparallel to the magnetic field, respectively, as found without SO coupling.

is easily polarized—taking values close to 1 $[\hbar/2]$. On the other hand, for **B** oriented along the wire, the $\langle s_B \rangle$ is around 0.885 $[\hbar/2]$. The amplitude of the oscillations depends on the nanowire radius [compare the curves in Fig. 3(a) for three values of R] and the oscillations are the strongest for a narrow

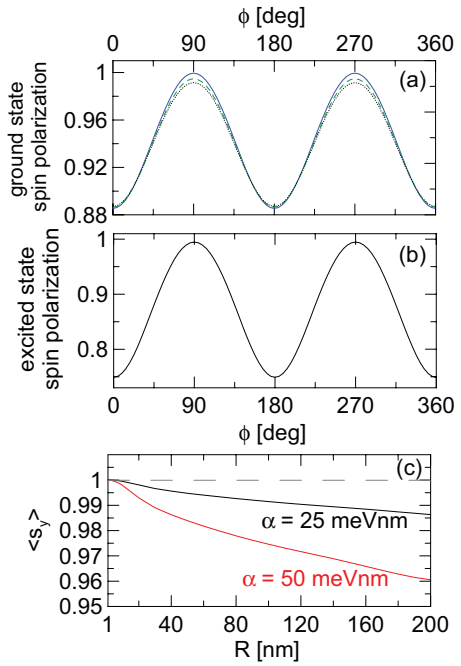

FIG. 3. (Color online) (a) Mean value of the spin along the magnetic field direction obtained for the ground state of the nanowire quantum dot with radius $R = 10$ nm (blue solid curve), $R = 50$ nm (green dashed curve), and $R = 100$ nm (black dotted curve). (b) Spin polarization of the second excited state for $R = 50$ nm. (c) Mean value of the spin-y component for the magnetic field aligned along the y direction as a function of the nanowire radius R. (a)–(c) are obtained for $B = 5$ mT. Results for $\alpha = 50$ meV nm correspond to $F_z = 100$ kV/cm.

nanowire with $R = 10$ nm. The spin polarization of the excited state is presented in Fig. 3(b). We observe that the amplitude of the oscillation is stronger than the one obtained for the ground state, but the spin polarization for $\phi = 90^\circ$ is again close to 1 $[\hbar/2]$.

Let us inspect the degree of the maximal spin polarization at the easy axis $\phi = 90^\circ$. In Fig. 3(c), we plot the mean value of the spin-y component of the ground state versus the wire radius R. We observe that as the wire becomes narrower, the spin polarization becomes almost complete (i.e., $1 - \langle s_y \rangle 2/\hbar < 10^{-4}$ for $R = 1$ nm) despite the presence of the SO coupling. The existence of directions in which the spin can be exactly polarized should facilitate the qubit initialization and increase the spin coherence times. On the other hand, as the wire becomes wider, the spin polarization drops with the slope of the curves in Fig. 3(c) depending on the SO coupling constant α. Note that the extent of the wave function in the z direction is limited also by the applied electric field.

When the magnetic field is increased, it splits the doublets—see the energy levels in Fig. 2. The energy splittings obtained for the magnetic field perpendicular to the nanowire axis (red curves in Fig. 2) are stronger than those obtained for the magnetic field parallel to the nanowire axis (black curves in Fig. 2). In the following, we explain this observation.

B. Asymptotic solution (1D limit)

When the wire becomes narrow the energy of the states excited in the radial direction rises. It is reasonable then to inspect the case in which the radial degrees of freedom are decoupled from the longitudinal one (the x direction). Such a system is described by the one-dimensional (1D) Hamiltonian,[24,25]

$$h_{1D} = \frac{\hbar^2 k_x^2}{2m^*} + V_L(x) - \alpha \sigma_y k_x + \frac{1}{2}\mu_B g B(\sigma_x \cos\phi + \sigma_y \sin\phi), \tag{8}$$

where $k_x = -i\frac{\partial}{\partial x}$.

Generally, the analytical solution for a SO coupled confined system are not known, with the exception of a special case of equal strength of Rashba and Dresselhaus coupling described in Ref. 21. Here we note, however, that in the absence of the magnetic field ($B = 0$) the Hamiltonian (8) commutes with the spin-y Pauli matrix and its eigenstates have definite y component of the spin. We find that for a quasi-one-dimensional nanowire, the spin orbitals (where N stands for the orbital quantum number and $\pm$ denotes the spin polarization of the state) have the form

$$\Psi_{N\pm} = \frac{1}{\sqrt{2}} \begin{pmatrix} 1 \\ \pm i \end{pmatrix} \varphi_N(x) \exp\left[\pm \frac{i\alpha m^*}{\hbar^2} x \right], \tag{9}$$

where $\varphi_N(x)$ are spin-independent eigenstates of Hamiltonian (8) for $\alpha = 0$ and $B = 0$. The eigenenergies of the Hamiltonian (8) are $E_{1D} = E_{\alpha=0,N} + E_{SO}$, where $E_{SO} = -\alpha^2 m^*/(2\hbar^2)$ is the energy shift to the whole energy spectrum introduced by the SO interaction[27] and $E_{\alpha=0,N}$ is an energy level of the Nth eigenstate obtained without SO coupling.

The magnetic field affects the energy levels of a strongly confined electron mainly through the Zeeman spin-splitting.

To investigate its influence on the SO eigenstates with an orbital excitation N, let us diagonalize h_{1D} for $B > 0$ in a basis consisting of a degenerate pair Ψ_{N+} and Ψ_{N-}. The Hamiltonian matrix is

$$\begin{pmatrix} \langle\Psi_{N+}|h_{1D}|\Psi_{N+}\rangle & \langle\Psi_{N-}|h_{1D}|\Psi_{N+}\rangle \\ \langle\Psi_{N+}|h_{1D}|\Psi_{N-}\rangle & \langle\Psi_{N-}|h_{1D}|\Psi_{N-}\rangle \end{pmatrix}, \tag{10}$$

where the diagonal elements are defined as follows:

$$\langle\Psi_{N\pm}|h_{1D}|\Psi_{N\pm}\rangle = E_{1D} \pm \tfrac{1}{2} g\mu_B B \sin\phi, \tag{11}$$

while the off-diagonal elements are

$$\langle\Psi_{N\pm}|h_{1D}|\Psi_{N\mp}\rangle = \mp i \frac{1}{2} g\mu_B B \int |\varphi_N|^2 \left[\cos\left(\frac{2\alpha m^*}{\hbar^2}x\right) \mp i \sin\left(\frac{2\alpha m^*}{\hbar^2}x\right)\right] \times dx \cos\phi. \tag{12}$$

Let us denote $\lambda_N \equiv \int |\varphi_N|^2 \cos(\frac{2\alpha m^*}{\hbar^2}x)dx$ and $\kappa_N \equiv i\int |\varphi_N|^2 \sin(\frac{2\alpha m^*}{\hbar^2}x)dx$.

The eigenstates of the matrix (10) are

$$E_{N\pm} = E_{1D} \pm \tfrac{1}{2} g\mu_B B\sqrt{1 - \left(1 - \lambda_N^2 + \kappa_N^2\right)\cos^2\phi}. \tag{13}$$

The energy difference between the states depends on the orientation of the magnetic field (angle ϕ) as well as the parameters λ_N and κ_N that control the strength of the anisotropy of the spin splittings for the rotated magnetic field. For the symmetric infinite quantum-well confinement along the wire (x direction), we obtain[29]

$$\lambda_1 = \frac{\hbar^6\pi^2 \sin(L\alpha m^*/\hbar^2)}{\alpha m^* L(\pi^2\hbar^4 - \alpha^2 m^{*2} L^2)} \tag{14}$$

and

$$\lambda_2 = \frac{4\hbar^6\pi^2 \sin(L\alpha m^*/\hbar^2)}{\alpha m^* L(4\pi^2\hbar^4 - \alpha^2 m^{*2} L^2)} \tag{15}$$

and $\kappa_1 = \kappa_2 = 0$ for the two lowest orbital states. The λ_N depends on the quantum dot length and the SO strength. In Fig. 4, we present the λ_1 parameter as a function of L and α.

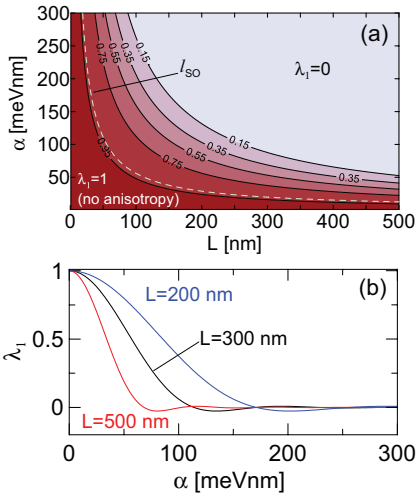

FIG. 4. (Color online) Parameter λ_1 as a function of the dot length L and SO coupling constant α. (b) Cross section of (a) for three different dot lengths L.

With the light-green dashed curve, we depict the SO length $l_{SO} = \hbar/(m^*\alpha)$. We observe that λ_1 drops quickly when the length of the dot becomes greater than the SO length. The shape of the λ_1 dependence on the SO strength for different quantum dot lengths is presented in Fig. 4(b), showing that the SO effects depend strongly on the quantum dot geometry and that λ_1 goes to 1 for vanishing SO coupling.

The smaller λ_N is, the stronger the SO coupling effects are. In particular, for the magnetic field parallel to the nanowire axis, the energy of the spin splitting is $E_S = g\mu_B B\lambda_N$. Consequently, the splitting can even go to 0 due to strong mixing of the spin states by the SO interaction [the light blue region in Fig. 4(a)].

When the magnetic field is aligned in the direction perpendicular to the nanowire axis, i.e., $\phi = 90^\circ$ or 270°, the off-diagonal elements of the matrix (10) vanish and the energy levels are split by Zeeman energy with the bulk value of the g factor. This is the reason for stronger spin splittings of the red curves in Fig. 2. For this configuration, the spin orbitals are separable into spin and orbital parts despite the presence of SO interaction and they have the exact form of Eq. (9). For any other orientation of the magnetic field, the off-diagonal elements mix the eigenstates (9). This results in decreasing the spin splittings by the SO interaction by an amount that depends on λ_N and κ_N parameters—the spatial extent of the wave function along the nanowire and the strength of the SO coupling. Moreover, the electron spin is no longer well defined as the electrons spin and orbital degrees of freedom are entangled.

We plot the energy spectrum obtained from Eq. (13) (shifted to match the energies obtained in the three-dimensional calculation at $B = 0$) with the crosses in Fig. 2. The spin splitting obtained from the one-dimensional model well describes the results of the three-dimensional calculation. The only discrepancy is visible for the energy levels of the first and the second excited states for $B > 100$ mT, which is due to mixing of these two states by the SO interaction.

As the magnetic field is rotated between the easy and hard axes, the spin polarization of the states changes, which results in changes of the spin-splitting strength. The latter term in Eq. (13) introduces Zeeman energy splitting between the energy levels of the two states. We can see that

$$g_N^* = g\sqrt{1 - (1 - \lambda_N^2 + \kappa_N^2)\cos^2\phi} \tag{16}$$

is an effective g factor that is dependent on the orientation of the magnetic field with the angle ϕ. With the crosses in Fig. 5(a) we plot the effective g factor as obtained from Eq. (16) along with the values obtained in the three-dimensional calculation (calculated as $g^* = \Delta E/\mu_B B$, where ΔE is the energy difference between the energy of the first excited state and the ground state—see Fig. 2) for different nanowire radii. For the nanowire radius $R = 10$ nm, the analytical solution and the result of the three-dimensional calculation match. For larger values of R, the shapes of the dependences comply, only the amplitude is different, with the biggest discrepancy being for the wide nanowire with $R = 100$ nm. The effective g-factor dependence obtained from the two excited states as calculated from Eq. (16) is plotted in Fig. 5(a) with circles. We observe

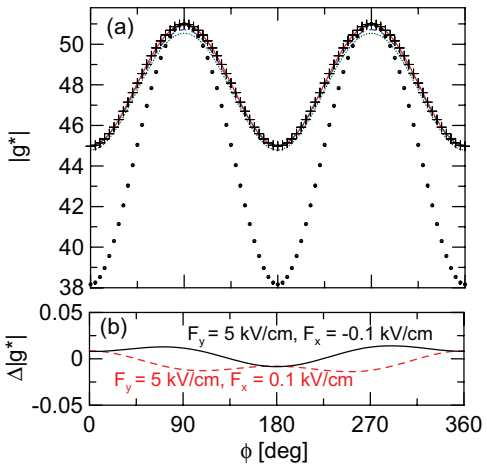

FIG. 5. (Color online) (a) Effective g factor obtained for a nanowire quantum dot with $R = 10$ nm (red solid curve), $R = 50$ nm (blue dashed curve), and $R = 100$ nm (green dotted curve) obtained for $B = 100$ mT. The symbols presents results obtained from Eq. (16) for the two lowest energy states $N = 1$ (black crosses) and for the second and third excited states $N = 2$ (black circles). (b) Difference between the g factor calculated for $F_x = F_y = 0$, $F_z = 50$ kV/cm, and calculated in the presence of the electric fields in the x and y directions as marked in the figure.

that due to the increased value of λ_2, the amplitude of the oscillation is greatly increased.

C. Additional SO terms

Additional external electric fields in the device that results from, e.g., a source and drain voltage difference or from gating of the nanowire, can activate additional terms of the Rashba Hamiltonian, which takes the general form

$$H_{\rm SO} = \alpha_0[F_x(\sigma_y k_z - \sigma_z k_y) + F_y(\sigma_z k_x - \sigma_x k_z) + F_z(\sigma_x k_y - \sigma_y k_x)]. \quad (17)$$

We inspect the influence of these additional terms on the anisotropic g factor including in addition to $F_z = 50$ kV/cm the electric field in the x direction (resulting from the bias voltage) and assuming the electric field in the y direction $F_y = 5$ kV/cm. Figure 5(b) presents the difference between results obtained with additional fields F_x, F_y and results obtained for only F_z present. Only slight differences are observed with the highest magnitude at the easy axes, i.e., $\phi = 90^\circ$ and 270°.

D. Two-electron results

The experimentally probed anisotropy of the g factor is extracted from the slopes of resonance lines in EDSR experiments on double quantum dots in the two-electron regime.[2,3] Figure 6(a) presents the two-electron energy spectrum of weakly coupled quantum dots defined in a nanowire with radius $R = 30$ nm obtained in the three-dimensional calculation. Results for the magnetic field oriented along the nanowire axis with $\phi = 0^\circ$ (perpendicular to the nanowire with $\phi = 90^\circ$) are plotted with solid (dotted) curves. The confinement potential includes now a potential barrier of 60 nm width that separates the electrons in adjacent dots both of

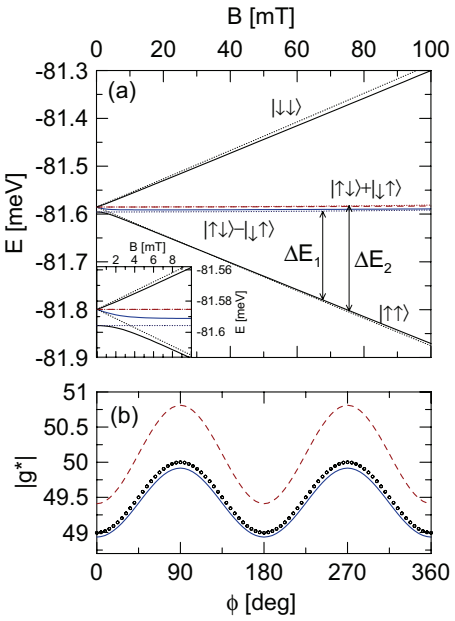

FIG. 6. (Color online) (a) Two-electron energy spectrum of coupled nanowire quantum dots with radius $R = 30$ nm. Solid curves present results for $\phi = 0^\circ$ and dotted curves for $\phi = 90^\circ$. With $|\uparrow\uparrow\rangle$, $|\downarrow\downarrow\rangle$, $|\downarrow\uparrow\rangle$, $|\uparrow\downarrow\rangle - |\downarrow\uparrow\rangle$, and $|\uparrow\downarrow\rangle + |\downarrow\uparrow\rangle$, we mark the spin configuration of the states parallel or antiparallel to the magnetic field as found without SO coupling. The inset presents the energy levels for low values of the magnetic field where the avoided crossing appears. (b) With the curves, the effective g factor is calculated from the energy splittings between the ground-state energy level and the energy levels depicted with blue solid (ΔE_1) and red dashed (ΔE_2) curves in (a) for $B = 200$ mT. The circles correspond to the effective one-electron g factor as obtained from Eq. (16) (shifted down by 1) for a single quantum dot with length $L = 120$ nm.

120 nm width. At $B = 0$, the ground state is a spin singlet ($|\uparrow\downarrow\rangle - |\downarrow\uparrow\rangle$) energy split from the degenerate triplet states [see the inset to Fig. 6(a)]. We tune the barrier height to 5 meV to match the singlet-triplet separation of $\simeq 5$ μeV as measured in Ref. 3.

At $B = 3$ mT, an avoided crossing between the two lowest energy levels appears for $\phi = 0^\circ$ due to spin mixing by the SO interaction. The width of the anticrossing is $\Delta E \simeq 8.2$ μeV, which is similar to the value measured in Ref. 3, i.e., $\simeq 5$ μeV. The experiment performed in Ref. 3 established that the anticrossing vanished for $\phi = 90^\circ$ and 270°, which is also the case in the present results—the anticrossing vanishes when the magnetic field orientation is parallel to the easy axes of the spin polarization.

After the anticrossing, the magnetic field splits the energy levels of the two spin-polarized triplet states ($|\uparrow\uparrow\rangle$ and $|\downarrow\downarrow\rangle$) by the Zeeman energy. The blue solid and red dashed curves in Fig. 6(a) whose energy does not change (after the anticrossing) with B are the singlet ($|\uparrow\downarrow\rangle - |\downarrow\uparrow\rangle$) and triplet ($|\uparrow\downarrow\rangle + |\downarrow\uparrow\rangle$) states with zero spin component in the direction along the magnetic field. Those levels are split by exchange interaction[25] (additional splitting of those two energy levels occurs when the g factor along the structure is not constant[2–4]).

The magnetic-field orientation (angle ϕ) (i) influences the strength of the spin polarization of the triplet states $|\uparrow\uparrow\rangle, |\downarrow\downarrow\rangle$ which results in a change of the slope of the corresponding energy levels, and (ii) changes in the exchange energy (spacing between energy levels of $|\uparrow\downarrow\rangle - |\downarrow\uparrow\rangle$ and $|\uparrow\downarrow\rangle + |\downarrow\uparrow\rangle$ states, plotted with blue solid and red dashed curves in Fig. 6(a). These two effects lead to a dependence of the effective g factor on ϕ which we calculate from the energy splittings between the ground state and the first and second excited states and plot in Fig. 6(b) with the blue solid and red dashed curves, respectively. We find that the shape of both curves in Fig. 6(b) matches the shape of the single-electron dependence presented in Fig. 5; only the amplitude of the oscillations is lower. As described by Eq. (16) for the single-electron case, the amplitude of g-factor oscillations depends on the dot length. In the present case, each of the coupled quantum dots has a length of $L = 120$ nm. The effective g factor obtained for a *single* dot of this length as calculated from Eq. (16) is plotted with circles in Fig. 6(b). Obtained oscillations have a similar amplitude to that obtained for the two-electron system. This suggest that the low amplitude in the two-electron case results from the fact that each electron resides in a separate dot and the shape of the oscillations is controlled mainly by the single-electron spin-polarization anisotropy process described previously.

The shape of the g-factor dependence is similar to the one obtained in the experiment performed in Ref. 3. In particular, an agreement is obtained in the context of the slight change of the oscillation amplitude of the red dashed and blue solid curves in Fig. 6(b). This difference in amplitudes is due to a modification of the exchange energy that separates the energy levels of the singlet ($|\uparrow\downarrow\rangle - |\downarrow\uparrow\rangle$) and triplet ($|\uparrow\downarrow\rangle + |\downarrow\uparrow\rangle$) states by the rotated magnetic field. However, the experimental dependence of the effective g factor is shifted (with minima at $\phi = 124^\circ$ and 304°) with respect to the present result. We performed calculations for quantum dots in a nanowire of larger radius ($R = 100$ nm) ruling out the possible orbital effects of the magnetic field as a reason for the shift. Also the additional terms of Rashba coupling operator are not responsible for such a shift, as discussed in Sec. III C. On the other hand, the g factor in quantum dots is affected by the local strain and asymmetries in the structure[30] which can influence the g factor as a concurrent process to the anisotropic spin polarization.

IV. SUMMARY AND CONCLUSIONS

In the present work, we studied the anisotropy of spin polarization in a narrow nanowire quantum dot in the presence of SO coupling. Solving the three-dimensional Schrödinger equation, we showed that the strength of spin polarization in the presence of Rashba SO interaction depends on the orientation of the magnetic field, and that there are hard and easy spin polarization axes. We explained the existence of these axes by the intrinsic tendency of SO coupling to polarize spins in the direction perpendicular to the nanowire. For the magnetic field aligned in this direction, the electron spin polarization can be nearly complete depending on the nanowire radius. We presented an analytical solution for the one-dimensional limit in which spin polarization can be complete, and we compared its results with the calculation for a finite thickness nanowire. Spin-polarization anisotropy results in an effective g-factor dependence on the magnetic-field orientation which is stronger for the excited states. The anisotropy of single-electron spin polarization results in changes of the avoided crossing width in the lowest part of the two-electron energy spectra. The magnitude and position of the extrema of this dependence match those founds in the experiment. Also, the form of the g-factor dependence resembles that obtained in the experimental studies.

ACKNOWLEDGMENTS

This work was supported by funds from the Ministry of Science and Higher Education (MNiSW) for 2012–2013 under Project No. IP2011038671, and by PL-Grid Infrastructure. M.P.N. is supported by the Foundation for Polish Science (FNP) scholarship under START and the MPD Programme cofinanced by the EU European Regional Development Fund.

[1] S. Nadj-Perge, S. M. Frolov, E. P. A. M. Bakkers, and L. P. Kouwenhoven, Nature (London) **468**, 1084 (2010).
[2] M. D. Schroer, K. D. Petersson, M. Jung, and J. R. Petta, Phys. Rev. Lett. **107**, 176811 (2011).
[3] S. Nadj-Perge, V. S. Pribiag, J. W. G. van den Berg, K. Zuo, S. R. Plissard, E. P. A. M. Bakkers, S. M. Frolov, and L. P. Kouwenhoven, Phys. Rev. Lett. **108**, 166801 (2012).
[4] S. M. Frolov, J. Danon, S. Nadj-Perge, K. Zuo, J. W. W. van Tilburg, V. S. Pribiag, J. W. G. van den Berg, E. P. A. M. Bakkers, and L. P. Kouwenhoven, Phys. Rev. Lett. **109**, 236805 (2012).
[5] C. Fasth, A. Fuhrer, L. Samuelson, V. N. Golovach, and D. Loss, Phys. Rev. Lett. **98**, 266801 (2007); A. Pfund, I. Shorubalko, K. Ensslin, and R. Leturcq, Phys. Rev. B **76**, 161308(R) (2007).
[6] Y. A. Bychkov and E. I. Rashba, J. Phys. C **17**, 6039 (1984).
[7] G. Dresselhaus, Phys. Rev. **100**, 580 (1955).
[8] K. C. Nowack, F. H. L. Koppens, Yu. V. Nazarov and L. M. K. Vandersypen, Science **318**, 1430 (2007).
[9] S. Datta and B. Das, Appl. Phys. Lett. **56**, 665 (1990).
[10] A. V. Khaetskii and Y. V. Nazarov, Phys. Rev. B **61**, 12639 (2000); V. N. Golovach, A. Khaetskii, and D. Loss, Phys. Rev. Lett. **93**, 016601 (2004); M. Florescu and P. Hawrylak, Phys. Rev. B **73**, 045304 (2006); S. Amasha, K. MacLean, Iuliana P. Radu, D. M. Zumbühl, M. A. Kastner, M. P. Hanson, and A. C. Gossard, Phys. Rev. Lett. **100**, 046803 (2008).
[11] Y. Yin, Semicond. Sci. Technol. **25**, 125004 (2010); M. Wang, Y. Yin, and M. W. Wu, J. Appl. Phys. **109**, 103713 (2011).
[12] K. V. Kavokin, Phys. Rev. B **64**, 075305 (2001); S. C. Badescu, Y. B. Lyanda-Geller, and T. L. Reinecke, *ibid.* **72**, 161304(R) (2005); S. Gangadharaiah, J. Sun, and O. A. Starykh, Phys. Rev. Lett. **100**, 156402 (2008).
[13] S. Takahashi, R. S. Deacon, K. Yoshida, A. Oiwa, K. Shibata, K. Hirakawa, Y. Tokura, and S. Tarucha, Phys. Rev. Lett. **104**, 246801 (2010).

[14]M. P. Nowak, B. Szafran, F. M. Peeters, B. Partoens, and W. J. Pasek, Phys. Rev. B **83**, 245324 (2011).
[15]M. P. Nowak and B. Szafran, Phys. Rev. B **83**, 035315 (2011).
[16]R. S. Deacon, Y. Kanai, S. Takahashi, A. Oiwa, K. Yoshida, K. Shibata, K. Hirakawa, Y. Tokura, and S. Tarucha, Phys. Rev. B **84**, 041302(R) (2011).
[17]H. A. Nilsson, P. Caroff, C. Thelander, M. Larsson, J. B. Wagner, L. E. Wernersson, L. Samuelson, and H. Q. Xu, Nano Lett. **9**, 3151 (2009).
[18]S. Roddaro, A. Fuhrer, P. Brusheim, C. Fasth, H. Q. Xu, L. Samuelson, J. Xiang, and C. M. Lieber, Phys. Rev. Lett. **101**, 186802 (2008).
[19]C. H. L. Quay, T. L. Hughes, J. A. Sulpizio, L. N. Pfeiffer, K. W. Baldwin, K. W. West, D. Goldhaber-Gordon, and R. de Picciotto, Nat. Phys. **6**, 336 (2010).
[20]V. Mourik, K. Zuo, S. M. Frolov, S. R. Plissard, E. P. A. M. Bakkers, and L. P. Kouwenhoven, Science **336**, 1003 (2012).
[21]J. Schliemann, J. C. Egues, and D. Loss, Phys. Rev. Lett. **90**, 146801 (2003).
[22]B. A. Bernevig, J. Orenstein, and S.-C. Zhang, Phys. Rev. Lett. **97**, 236601 (2006).
[23]J. D. Koralek, C. P. Weber, J. Orenstein, B. A. Bernevig, S.-C. Zhang, S. Mack and D. D. Awschalom, Nature (London) **458**, 610 (2009).
[24]Y. V. Pershin, J. A. Nesteroff, and V. Privman, Phys. Rev. B **69**, 121306(R) (2004); C. Flindt, A. S. Sorensen, and K. Flensberg, Phys. Rev. Lett. **97**, 240501 (2006); J. Phys.: Conf. Ser. **61**, 302 (2007).
[25]M. P. Nowak and B. Szafran, and F. M. Peeters, Phys. Rev. B **86**, 125428 (2012).
[26]O. Voskoboynikov, C. P. Lee, and O. Tretyak, Phys. Rev. B **63**, 165306 (2001); C. F. Destefani, S. E. Ulloa, and G. E. Marques, *ibid.* **69**, 125302 (2004).
[27]The obtained energy shift is twice as small as the one obtained for two-dimensional systems in Ref. 28.
[28]M. Valín-Rodríguez, A. Puente, and L. Serra, Phys. Rev. B **69**, 085306 (2004).
[29]In general, the form of λ_N and κ_N can be provided for any confinement potential for which the analytical form of the wave functions is known, in particular for the harmonic-oscillator potential.
[30]C. E. Pryor and M. E. Flatté, Phys. Rev. Lett. **96**, 026804 (2006).